Three-dimensional instabilities for the flow around a heaving foil

Liping Sun, Jian Deng,* and Xueming Shao
Key Laboratory of Soft Machines and Smart Devices of Zhejiang Province, Zhejiang University, Hangzhou 310027, P. R. China and Department of Mechanics, Zhejiang University, Hangzhou 310027, P. R. China

(Received 18 October 2017; published 22 January 2018)

This paper investigates the three-dimensional instabilities of the flow past a periodically heaving airfoil. By comparison with a pitching foil [Deng *et al.*, Phys. Rev. E **92**, 063013 (2015)], here we present distinctive characteristics for the heaving foil, particulary regarding its Floquet modes. By increasing the frequency (Sr), or equivalently decreasing the amplitude (A_D) along the marginal stability curve in the (Sr, A_D) phase space, the critical Floquet mode emerges sequentially as A, quasiperiodic (QP), and B. It is interesting to note that both modes A and B are synchronous with the base flow, in contrast to the quasiperiodic mode QP. To further investigate the instability across the marginal curve, we fix the frequency at $\mathrm{Sr} = 0.187$, of which the critical Floquet mode is located in the synchronous regime, while varying A_D around the critical point. We find that the dominant mode switches from mode A to mode B, while mode QP never becomes critical as we increase A_D. We note that mode S, a subharmonic mode, can also be unstable, which, however, is not physically realizable, because the magnitude of its Floquet multiplier is always smaller than that of mode B. We have also studied the influence of various Reynolds numbers at the same critical point on the marginal stability curve, with the results resembling that by varying the amplitude A_D.

DOI: 10.1103/PhysRevE.97.013110

I. INTRODUCTION

In recent years, the development of micro air vehicles and small unmanned underwater vehicles has led to a growing interest in aerodynamics and hydrodynamics of flapping wings [1–7]. It is well known that most insects and birds flap their wings in a so-called stroke plane employing a combination of rotation with respect to the wing-body junction and pitching with respect to the spanwise axis. As a rational simplification, researchers have been restricting their attention to two-dimensional (2D) airfoil configurations with the combination of a vertical oscillation, so-called heaving or plunging, and a rotation with respect to a pivoting point, so-called pitching. An important parameter used in the study of flapping wings is the Strouhal number, defined as $\mathrm{Sr}_A = fA/U$, where f is the flapping frequency and A is the amplitude. Sr_A characterizes the wake dynamics, thus the propulsive performance of a flapping foil. The cruise Strouhal numbers for a wide range of flying and swimming animals lie within a narrow interval $0.2 < \mathrm{Sr}_A < 0.4$ [3], suggesting that natural selection has tuned animals for high propulsive efficiencies [8,9].

The quasi-two-dimensional hypothesis is invalid when the aspect ratio of the wing is small. Thus there have been many studies on flapping wings with finite aspect ratio [10–13]. However, even in the situation of infinite aspect ratio, 3D instabilities might develop and lead to modifications of the flow around the flapping foil and, consequently, to modifications of the hydrodynamic forces. Recently, the Floquet stability analysis has been used to study the three-dimensional transition in the wake of a pitching foil [14,15], as well as that of a flapping foil with combined motions [16]. In Ref. [15], a pitching NACA0015 airfoil was considered at a fixed Reynolds number $\mathrm{Re} = 1700$. It was reported that the transition from a 2D wake to a 3D wake occurred always after when the wake was deflected. Two distinct unstable modes were identified, of which the subdominant long-wavelength mode, which is not physically realizable, has certain points of similarity with the so-called mode A for a circular cylinder [17,18], while the short-wavelength mode appears to have a period of the order of twice that of the base flow, which was conjectured to be a subharmonic mode (mode S), and is dominant and physically realizable. In Ref. [16], four cases were studied for a pitching and heaving NACA0012 airfoil at $\mathrm{Re} = 1000$. At a specific case, a linearly unstable mode was found to occur in the range of wavelength $2.24 \leqslant \lambda/c \leqslant 6.7$, with the Floquet multiplier peaking at $\lambda/c = 4.078$, which was identified as a mode A instability.

So far, as we have known [14,15,19,20], for the wake behind a flapping foil it is possible to divide the (Sr, A_D) phase space into different regimes by three boundaries: first, the transition from the well-known Bénard-von Kármán (BvK) wake to the reversed BvK vortex street that signals propulsive wakes; second, the symmetry breaking of this reverse BvK pattern giving rise to an asymmetric or deflected wake; and, third, a further transition from a 2D wake to a 3D wake. It has been long established that the reverse BvK vortex street was an indication of thrust generation [8,21]. This statement has been corrected later whereby the reversal of the vortex street occurs actually before the drag-thrust transition in almost all cases except for the high flapping frequencies in the (Sr, A_D) phase space [15]. The deflection of the wake has also been extensively studied, exhibiting that the clockwise and counterclockwise trailing edge vortices shed in pairs and propagate at an angle to the

*Corresponding author: zjudengjian@zju.edu.cn

streamwise axis [19,20,22,23]. The wake can be deflected to either the lower side or upper side of the wake center line, so-called dual modes. The deflected direction largely has been recognized to depend on the initial flapping conditions [24,25]. Also, small disturbances could trigger the switch between the modes in a random fashion [26,27]. Recently, a perturbation analysis method was adopted to investigate the wake deflection behind a pure pitching foil [28]. A Floquet stability analysis of the time-periodic nondeflected wake showed that there exists a synchronous antisymmetric mode which becomes unstable at the critical flapping frequency where deflection occurs. To our knowledge, the third transition boundary, i.e., the 2D-3D transition for a flapping foil, has rarely been studied until the recent research on a pure pitching foil [14,15].

The wake dynamics behind a pure pitching foil and that of a pure heaving foil could be different, and thus they have usually been studied separately [29]. Recently, a direct comparison was made between a flapping foil with a pure pitching motion and that with a pure heaving motion [30]. It was reported that at a fixed Reynolds number, Re = 1700 (Re = Uc/ν, where c is the chord length and ν is the kinematic viscosity of the fluid), the drag-thrust transition took place approximately at $\mathrm{Sr}_A = 0.22$ for the pure pitching foil, and the drag-thrust transition for a pure heaving foil also closely followed an Sr_A contour line, albeit at the lower value $\mathrm{Sr}_A = 0.14$. This correlation between the drag-thrust transition and the Sr_A has also be studied by experiments, which were carried out in a soap film tunnel [29]. Two critical Strouhal numbers, $\mathrm{Sr}_A = 0.28$ and $\mathrm{Sr}_A = 0.16$, were found to match the drag-thrust transitions for respectively the pure pitching and the pure heaving foils.

It is not surprising to expect that the wake of a heaving foil might respond differently to three-dimensional spanwise periodic perturbations, in contrast to a pitching foil. In Ref. [15], we have drawn a comprehensive map on the (Sr, A_D) phase space, with two typical unstable modes identified. In this paper, by following the similar hierarchy of analysis engaged in Ref. [15], we aim to perform a parametric study of three-dimensional instabilities in the wake of a heaving foil. We focus on the sequential emergences of different instability modes as we vary the parameters, such as the heaving amplitude, the frequency, or the Reynolds number [14].

II. PROBLEM FORMULATION AND COMPUTATIONAL METHODS

A. Foil kinematics and dimensionless parameters

We consider a NACA0015 airfoil experiencing simultaneous heaving motion with a sinusoidal profile, as shown in Fig. 1, and can be expressed as

$$h(t) = h_0 \sin(2\pi f t), \tag{1}$$

where h_0 is the amplitude of heaving motion and f is its frequency. The peak-to-peak amplitude of the trailing edge is denoted by A, where $A = 2h_0$. We define the Reynolds number Re = Uc/ν, where c is the chord length, U is the streamwise velocity far upstream, and ν is the kinematic viscosity. The two parameters which characterize the wake dynamics are the appropriately scaled amplitude A_D and frequency or, equivalently, the Strouhal number S_r, defined respectively as

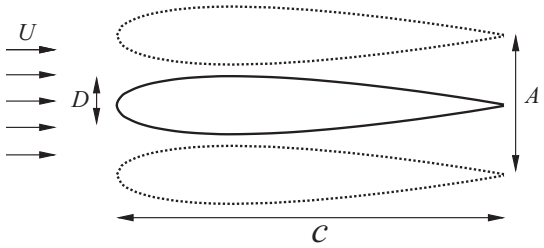

FIG. 1. Schematic view of the foil profile, which is symmetric, heaving with the peak-to-peak amplitude A. D denotes the thickness of the foil, which is $0.15c$ for a NACA0015 airfoil.

$$A_D = A/D \quad \text{and} \quad \mathrm{Sr} = fD/U. \tag{2}$$

Another alternative Strouhal number, which has been widely used to characterize the wake produced by a biomimic flapping foil, is defined as

$$\mathrm{Sr}_A = fA/U. \tag{3}$$

We choose Re = 1700 for most of the following simulations, which is consistent with the previous studies [15,19], and we understand that at this intermediate Reynolds number, clear wake transitions can be observed in the amplitude-frequency parametric space covered by our studies.

B. Modelling the base flow

The base flow is governed by the two-dimensional incompressible Navier-Stokes and continuity equations. The numerical simulations is mainly performed using the finite-volume method [31]. The mass and momentum equations are solved on a moving grid domain using the arbitrary Lagrangian Eulerian (ALE) formulation. For a heaving foil, the whole domain moves along with the foil. The integral form of the governing (conservation) equations defined in an arbitrary moving volume V bounded by a closed surface S is

$$\frac{d}{dt}\int_V \rho \mathbf{U} dV + \oint_S \mathbf{ds}\cdot\rho(\mathbf{U}-\mathbf{U}_b)\mathbf{U} = \oint_S \mathbf{ds}\cdot(-p\mathbf{I}+\rho\nu\nabla\mathbf{U}), \tag{4}$$

where ρ is the fluid density, $\mathbf{U}$ is the fluid velocity, $\mathbf{U}_b$ is the boundary velocity of a cell, p is the static pressure, and ν is the kinematic viscosity. For the discretization and implementation of boundary conditions, one can refer to Ferziger and Peric [32] for details.

The space discretizations are second-order upwind for the convection terms and central differences for the Laplacian terms, respectively. The temporal discretization is second-order implicit Euler. The pressure-velocity coupling is obtained using the pressure-implicit with splitting of operator (PISO) scheme [32]. The preconditioned conjugate gradient (PCG) method is used to treat the pressure equation and the preconditioned biconjugate gradient (PBiCG) method is used for the velocity equations. Numerical accuracy is set to double precision and the initial conditions are chosen to be uniform. We set the boundary condition on the foil to be moving wall,

with no flux normal to the wall. A constant velocity is imposed on the inlet boundary, and the pressure at the outlet boundary is set to a constant value.

The computational domain is a rectangle, of which the dimensions of its outer boundary is $20c \times 18c$. A mesh of about 200 000 cells is used for the calculations. The same solver has been validated in Ref. [15], in which a pitching foil with prescribed motions was studied.

C. Floquet stability analysis

Floquet stability analysis can be used to determine the stability of the periodic symmetric base flow to asymmetric perturbations. By introducing a perturbation spanwise wave number $\beta = 2\pi/\lambda_z$, where λ_z is the spanwise wavelength of the disturbance, we can approximate the perturbation velocity and pressure as a sum of Fourier modes in the spanwise direction. Each mode of the perturbation field can then be integrated forward in time within our linearized approximation directly using the same algorithm used for the base flow and renormalized at the end of each base flow period. According to Floquet theory [33,34], only the dominant Floquet mode remains after many cycles. Here we measure the Floquet multiplier $|\mu|$ as the ratio of the current L_2 norm of any of the velocity perturbations to the L_2 norm exactly one period prior. If $|\mu| > 1$, then the corresponding perturbation field grows exponentially from one period to the next and hence the base flow is linearly unstable to perturbations of the selected spatial wavelength in the z direction. Conversely, if the multipliers for all possible wave number β are less than unity, the base flow is stable. For $|\mu| = 1$, the base flow is neutrally stable, where the imposed perturbation neither grows nor decays. The implementation of the method in this case is similar to that of Barkley and Henderson [35]. Effectively, the perturbation field satisfying the linearized Navier-Stokes equations is evolved at each time step in parallel to the base flow. The present numerical technique has been successfully applied to various problems [36–39]. (More technical details about Floquet stability analysis and its application to a flapping foil are presented in Refs. [14,15].)

III. RESULTS

A. Flow regimes within the (Sr, A_D) phase space

To identify the different regimes for the flow around a heaving foil, we perform a parametric study at a fixed Reynolds number Re = 1700, with varying Sr and A_D. In Fig. 2, three distinct transition boundaries are found in the (Sr, A_D) phase space: the transition from a well-known BvK vortex street to a reverse BvK vortex street, the transition from a symmetric flow wake (with respect to the wake center line) to a deflected wake, and a further transition from a 2D wake to a 3D wake.

We note that the third transition boundary (red dash-dot-dot line in Fig. 2) is a neutral stability curve on which the maximum magnitude of Floquet multipliers over the range of β equals to unity. It is not surprising that the 2D-3D transition boundary lies to the top right of the boundary between the reverse BvK streets and the deflected wakes, implying that the 2D-3D transition occurs after the wake deflection, which has also be found for a pitching foil [15]. The difference is

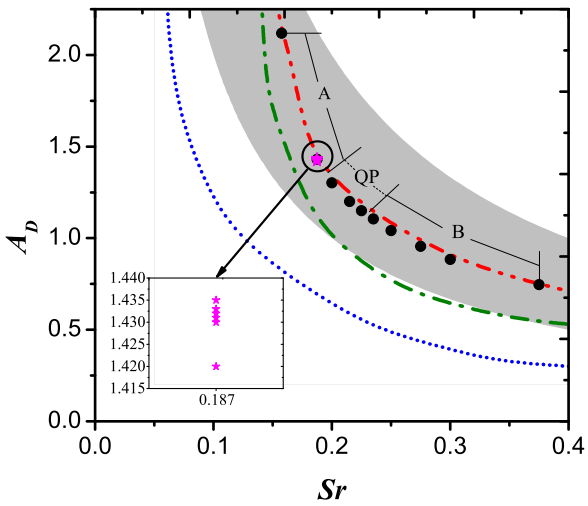

FIG. 2. A_D vs. Sr map for Re = 1700. Red (dash-dot-dot) line: the curve of marginal three-dimensional stability or the transition boundary from 2D to 3D flows, with computational points labeled as stars and dots for further discussion. Blue (dotted) line: transition between BvK and reverse BvK wakes. Green (dash-dot) line: transition from symmetric to asymmetric wakes with respect to the wake center line. The shaded area corresponds to the $\mathrm{Sr}_A = 0.2-0.4$ interval.

that the 2D-3D transition boundary for a heaving foil stays closer to the wake deflection boundary in contrast to that for a pitching foil. For more comparisons between pitching and heaving foils, particularly in their propulsive performance, one can refer to the previous paper [30], which is, however, not the main scope of the current study. In the follow discussion, we focus specifically on the instabilities for a heaving foil, depicted primarily by the Floquet modes in the neighborhood of its marginal stability curve.

B. Floquet modes on the marginal stability curve

In Fig. 2, we have determined that there is a single curve of marginal stability for the breaking of the spanwise translation invariance, or 2D-3D transition. By examining these Floquet modes, we find that there are two distinct types of behavior, depending on whether the critical Floquet multipliers are real and positive or occur in complex-conjugate pairs. As we have discussed in Ref. [40], it is possible to distinguish these two different modes by studying the time history of the Floquet multiplier $|\mu|$. We integrate both the numerical simulation (NS) equations and the linearized equations forward in time over several base flow periods T, until $|\mu|$ reaches a constant value, suggesting that the Floquet multiplier is real or fluctuates periodically around a constant value, suggesting that it also has an imaginary component. Moveover, if the oscillation of $|\mu|$ suggests that it has a secondary period $T_s = 2T$, i.e., the bifurcation solutions are period doubled or subharmonic. To further distinguish the subharmonic mode from the quasiperiodic mode, we can examine the evolution of the perturbation vorticity field.

We select several calculated points approximately on the marginal curve, marked with dots in Fig. 2. The variation of the Floquet multipliers with β for these critical points are

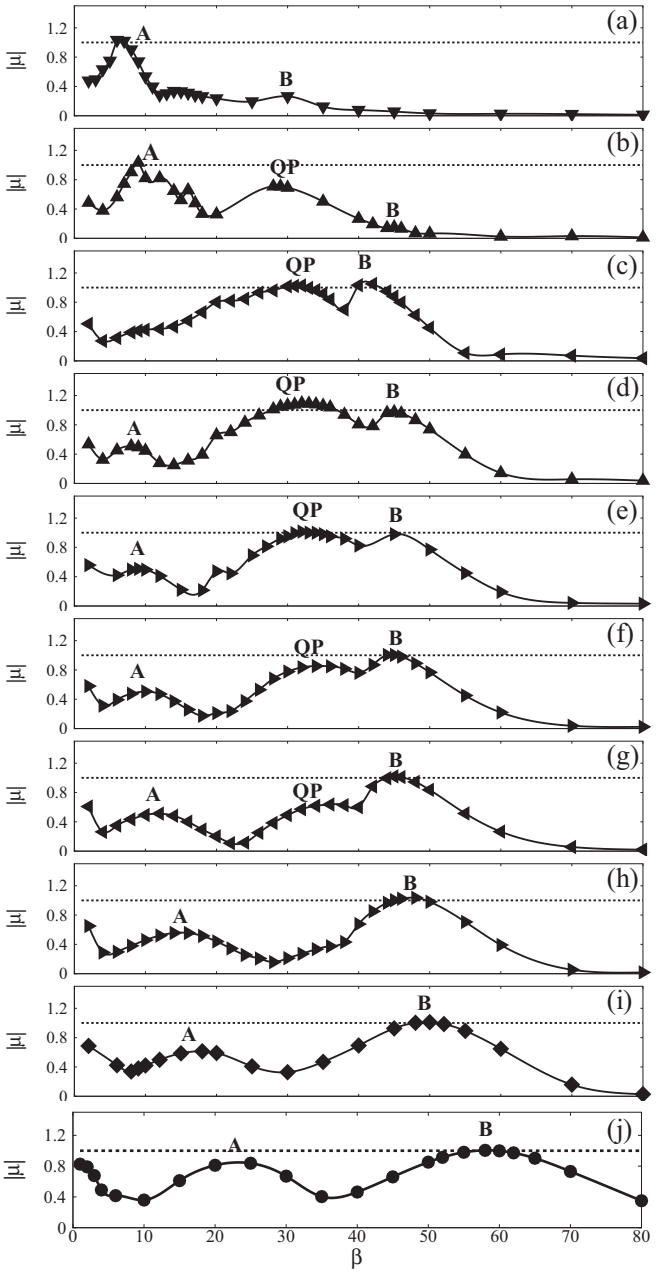

FIG. 3. Variation of Floquet multiplier magnitude $|\mu|$ with wave number β at Re = 1700 for different (Sr, A_D): (a) (0.157,2.118), (b) (0.187,1.431), (c) (0.200,1.303), (d) (0.215,1.200), (e) (0.225,1.150), (f) (0.235,1.105), (g) (0.250,1.042), (h) (0.275,0.955), (i) (0.300,0.884), and (j) (0.375,0.747). The line $|\mu| = 1$ corresponds to a neutral stability line.

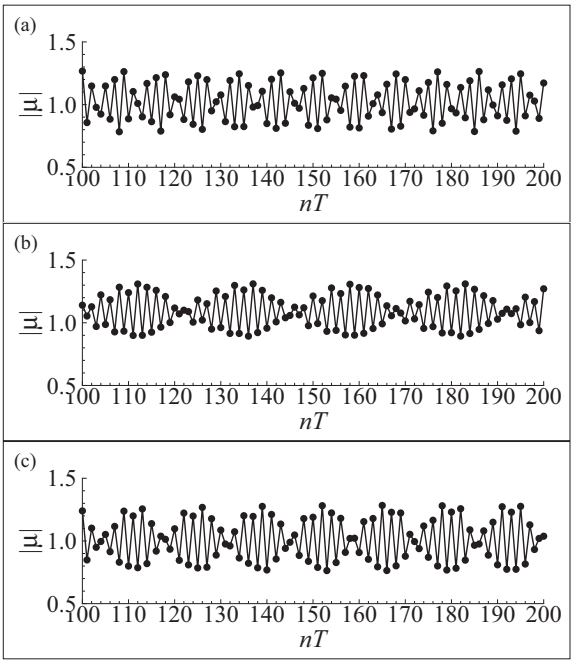

FIG. 4. Time histories of $|\mu|$ for the Floquet modes. (a) (Sr, A_D) = (0.200,1.303), (b) (Sr, A_D) = (0.215, 1.200), and (c) (Sr, A_D) = (0.225, 1.150) correspond to Fig. 3(c), 3(d) and 3(e), respectively.

shown in Fig. 3. As we increase Sr along the marginal curve, the critical Floquet mode emerges sequentially as mode A, mode quasiperiodic (QP), and mode B. For example, as shown in Fig. 3(a) for Sr = 0.157, the mode A instability, which is synchronous (with respect to the base flow), becomes critical at $\beta = 6$ or with a wavelength $\lambda/c = 1.05$. Mode QP becomes critical for Sr in the range of 0.200–0.225, with the wave number $\beta = 28-32$, as shown in Figs. 3(c)–3(e). We note that within this quasiperiodic regime, the peak values of $|\mu|$ for mode B are also very close to the neutral line, though slightly lower than that of mode QP. As Sr increases to 0.235, mode B appears to be the first to become critical. The corresponding wave number increases from $\beta = 45$ to $\beta = 60$ as Sr increases from Sr = 0.235 to Sr = 0.375, as shown in Figs. 3(f)–3(j). We note that mode B is also synchronous with the base flow.

If we write the Floquet multiplier as a complex number, $\mu = |\mu|e^{\pm i\theta}$, then we can obtain a complex-conjugate pair for the QP modes, corresponding to a Neimark-Sacker bifurcation which introduces the secondary period, $T_s = 2(\pi/\theta)T$, where T is the period of the base flow. It is also possible to obtain the secondary period T_s by examining the $|\mu|$ time history, as shown in Fig. 4. The secondary periods for the critical QP modes in Figs. 3(c), 3(d) and 3(e) are $T_s = 9T$, $T_s = 23T$, and $T_s = 14T$, respectively. It is interesting to compare the current study with the primary instabilities of the flow generated by an oscillating circular cylinder in quiescent fluid [41,42], in which the marginal stability curve within an amplitude-frequency control space was divided into two regimes labeled with "S" and "QP," representing synchronous and quasiperiodic instabilities, respectively. They identified a transition point, at which location the quasiperiodic mode "freeze" into a synchronous one. Similarly, in the current study, we can identify two transition points, Sr_f^+ and Sr_f^-, at which points the instability modes transit between synchronous and quasiperiodic modes. The exact transition points are possible to identify, which requires more calculated points along the marginal stability curve but is not the main concern of the current study. It is reasonable to compare the current study with Refs. [41,42], because the current configuration can be regarded as an oscillating foil superposed by a uniform incoming flow. We also note that it is significantly different between the previous [41,42] and the current studies. In Ref. [41] two-dimensional instability was considered, which breaks the

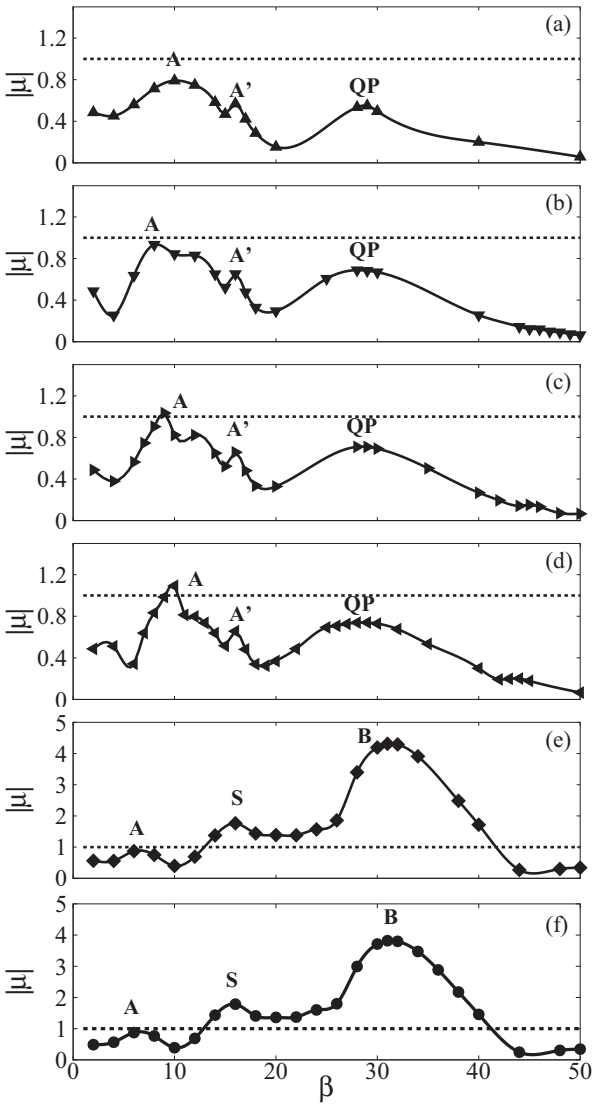

FIG. 5. Variation of Floquet multiplier magnitude $|\mu|$ with wave number β at Re = 1700 and Sr = 0.187 for different A_D: (a) 1.420, (b) 1.430, (c) 1.431, (d) 1.432, (e) 1.433, and (f) 1.435. The line $|\mu| = 1$ corresponds to neutral stability of the Floquet modes.

left-right symmetry of the flow induced by an oscillating circle, with a restriction to a two-dimensional subspace, while the current study considered the secondary instability, which breaks the spanwise translation invariance of a foil with an infinite span length. Further discussions about the different types of instabilities in terms of their symmetries and flow structures will be made in the following sections.

C. Effects of A_D on the instabilities

To examine how the flow becomes unstable when across the marginal stability curve, in Fig. 5 we present the variation of $|\mu|$ with spanwise wave number β for different A_D at Re = 1700 and Sr = 0.187. By increasing A_D, as it reaches $A_D = 1.431$, mode A becomes critical, as shown in Fig. 5(c). As we further increase A_D to $A_D = 1.432$, mode A becomes the only unstable mode [Fig. 5(d)]. It is interesting to find that both mode S and mode B appear to be unstable, as we increase A_D to $A_D = 1.433$, as shown in Fig. 5(e). In Fig. 5(e), mode B is the dominant mode with the maximum amplitude of Floquet multiplier, occurring at $\beta = 31$, and the other unstable mode, mode S, which is subharmonic, occurs at $\beta = 16$, while the third one, mode A, stays below the neutral line. This sequence of mode emergence is similar to that for the flow around a square cylinder [38]. It is interesting to note that before mode S becomes unstable the Floquet mode appears to be mode A′, which resembles mode A while at a different wave number, as shown in Figs. 5(a)–5(d).

As we have known that the T-periodic base flow, such as a BvK vortex street, obeys a reflectional symmetry about the wake centerline ($y = 0$) after a translation along the time axis whereby a half-period. Here we refer to this reflection-translation symmetry as RT symmetry for short. For mode A, each perturbation velocity component has the same symmetry as the two-dimensional base flow. Therefore, the streamwise vorticity for mode A obeys an odd RT symmetry expressed by

$$\widetilde{\omega}_x(x,y,z,t) = -\widetilde{\omega}_x(x,-y,z,t+T/2). \tag{5}$$

By contrast, for mode B, the velocity components display a RT symmetry; thus mode B obeys an even RT symmetry, and the corresponding expression of the streamwise vorticity is

$$\widetilde{\omega}_x(x,y,z,t) = \widetilde{\omega}_x(x,-y,z,t+T/2). \tag{6}$$

Therefore, according to these properties, we can distinguish mode A instability from mode B instability.

As for mode QP and mode S, which are not T periodic (as presented in Ref. [43]), we can distinguish them from the regular modes or T-periodic modes (mode A and mode B), which have Floquet multipliers containing only a positive real component and the time variation of $|\mu|$ maintain constant. Instead, the mode QP arises from a complex-conjugate pair of multipliers with a nonzero imaginary part. For mode S, the Floquet multipliers have only a negative real component, and the structure of the streamwise vorticity repeats over two base-flow periods. Therefore, the vorticity has a temporal symmetry represented as:

$$\widetilde{\omega}_x(x,y,z,t) = -\widetilde{\omega}_x(x,y,z,t+T). \tag{7}$$

Accordingly, we can make a distinction between mode QP and mode S.

To study the characteristics of these modes, we consider a specific case at Sr = 0.187 and $A_D = 1.433$ for Re = 1700, of which the Floquet multipliers are shown in Fig. 5(e). At this point we have identified one stable mode, mode A, and two unstable modes, mode S and mode B. We present their respective perturbation streamwise vorticities in Figs. 6–8 with $\beta = 6$ ($\lambda/c = 1.05$), $\beta = 16$ ($\lambda/c = 0.393$), and $\beta = 32$ ($\lambda/c = 0.196$), respectively.

Figure 6 shows the streamwise vorticity of the instability mode A, which is very similar in characteristics to that for the flow around a cylinder. As seen from Figs. 6(a)–6(e), it is clearly shown that this mode is T periodic, with the streamwise vorticity changing its sign every half-period about the wake center line. Figure 6(f) shows the time variation of $|\mu|$, indicating that the dominant mode has been isolated in the perturbation field 35 cycles after its initialization. The constant $|\mu|$ means that mode A contains no imaginary component, which implies a synchronous bifurcation.

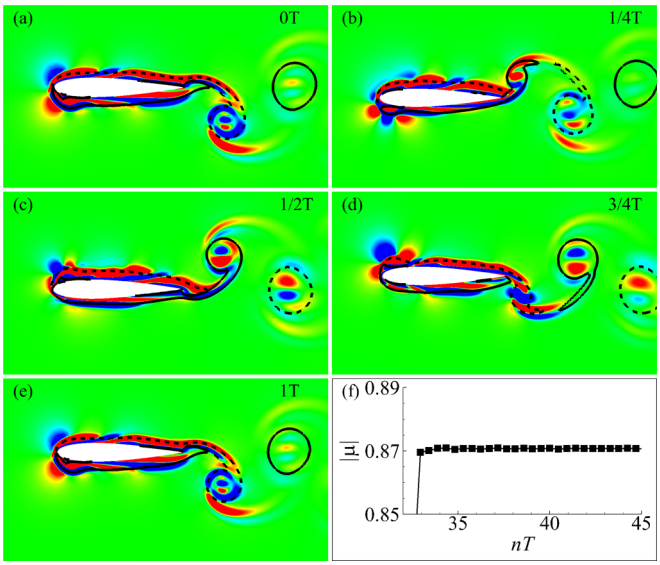

FIG. 6. [(a)–(e)] Instantaneous streamwise perturbation vorticity for mode A of the flow past a heaving foil at Re = 1700 for (Sr, A_D) = (0.187, 1.433) and $\beta = 6$. Blue (dark gray) and red (light gray) colors denote negative values and positive values, respectively, for continuous contour levels from −6 to 6. Spanwise vorticity contours of the base flow are also shown with solid and dashed lines for positive and negative values, respectively. (f) Time variation of $|\mu|$.

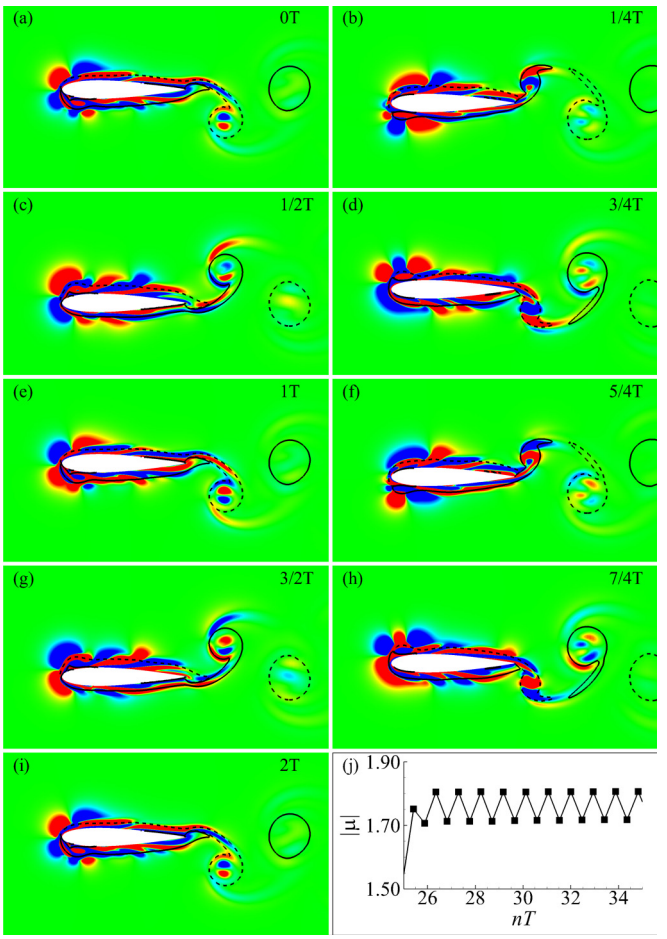

FIG. 7. [(a)–(i)] Instantaneous streamwise perturbation vorticity for mode S of the flow past a heaving foil at Re = 1700 for (Sr, A_D) = (0.187, 1.433) and $\beta = 16$. Blue (dark gray) and red (light gray) colors denote negative values and positive values, respectively, for continuous contours levels from −6 to 6. Spanwise vorticity contours of the base flow are also shown with solid and dashed lines for positive and negative values, respectively. (j) Time variation of $|\mu|$.

Figure 7 shows the streamwise vorticity of the instability mode S, in which we plot a series of streamwise perturbation vorticities taken $1/4T$ periods apart. It is evident that the perturbation vorticity field for this mode is not T periodic. It is apparent that the streamwise vorticity of the flow field repeats every period but with a sign change. The oscillating Floquet multiplier $|\mu|$ shown in Fig. 7(j) indicates that this mode has the secondary period $T_s = 2T$, i.e., the bifurcated solutions are period doubled or subharmonic, which also implies that this mode has only a negative real part. Therefore we can distinguish it from mode QP, which arises from a complex-conjugate pair of multipliers with a nonzero imaginary part.

In Fig. 8, we plot the streamwise perturbation vorticity of the instability mode B. Seen from Fig. 8(a)–8(e), it is apparent that mode B is also T periodic. However, unlike the vorticity plot of mode A which changes its sign every half-period about the wake center line, for mode B, the streamwise vorticity repeats every half-period on the other side of the wake centerline. The constant Floquet multiplier $|\mu|$ shown in Fig. 8(f) indicates that this mode contains no imaginary component and only has a positive real part, which also implies synchronous with respect to the base flow.

To illustrate the characteristics of mode QP, we consider a specific example and plot its wake topology in Fig. 9 for Sr = 0.187, $A_D = 1.432$, at Re = 1700 with the spanwise wave number $\beta = 29$, corresponding to a wavelength $\lambda/c = 0.217$. We note that although the mode QP is stable at this point, it is still interesting to examine the characteristics of this mode and make comparisons with the others. Figures 9(a)–9(p) show a series of images of the perturbation field taken one base-flow period apart. The series of images span approximately the secondary period of the Floquet multiplier oscillation. We observe that the perturbation vorticity field for this mode is not quite periodic due to the gradual growth and decay of the perturbation field on a much longer time scale. This is highlighted, for instance, by focusing on the initially positive region of perturbation vorticity inside the vortex at the immediate rear of the foil in the first image at $0T$. By scanning through the images, the perturbation vorticity field experiences a series of growth, weakens, and eventually repeats at $15T$. This illustrates that the mode is truly quasiperiodic and the structure of streamwise perturbation vorticity of the flow field repeats every 15 base-flow periods. Moreover, as shown in Fig. 9(q), the Floquet multiplier $|\mu|$ is seen to oscillate over time with a secondary period $T_s = 15T$, consistent with the evolution of the perturbation field.

To get a better understanding of the inherent three-dimensionality of these modes, we rebuild the three-dimensional perturbed flow fields, with their streamwise vorticities shown in Fig. 10. Since the amplitude is arbitrary due to it being a linear (and hence infinitesimal) perturbation, we rescale the vorticity field with its instantaneous maximum

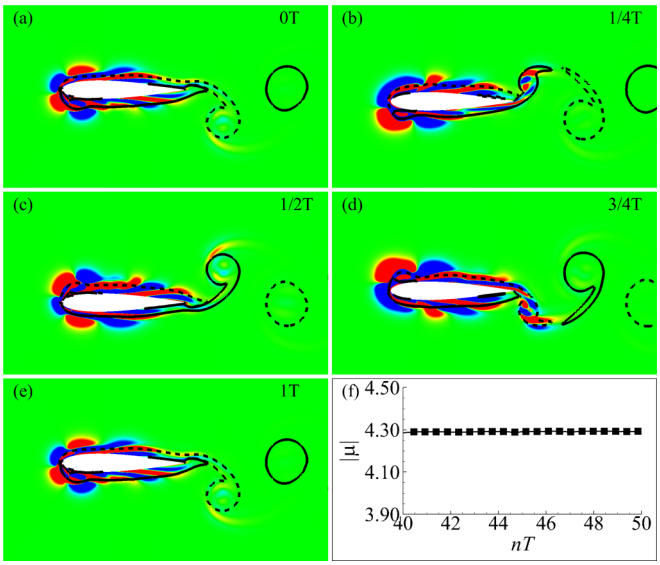

FIG. 8. [(a)–(e)] Instantaneous streamwise perturbation vorticity for mode B of the flow past a heaving foil at Re = 1700 for (Sr, A_D) = (0.187,1.433) and $\beta = 32$. Blue (dark gray) and red (light gray) colors denote negative values and positive values, respectively, for continuous contours levels from −6 to 6. Spanwise vorticity contours of the base flow are also shown with solid and dashed lines for positive and negative values, respectively. (f) Time variation of $|\mu|$.

value, similarly to the approach used in Figs. 6–9. For each representation, the spanwise domain is defined as $3\lambda_z$, allowing three wavelengths to be observed in the spanwise direction for each mode to fit inside the domain. In addition to the observed spatiotemporal symmetries of these modes, we note that for the high β number [see Fig. 10(c)], the perturbed streamwise vorticities cluster around the foil, instead of distributing in the flow wake [see Fig. 10(a)].

D. Effects of Reynolds number on the instabilities

To further explore how the flow becomes unstable under the effects of Reynolds numbers, in Fig. 11 we plot the variation of the Floquet multiplier magnitude $|\mu|$ with spanwise wave number β for various Re at Sr = 0.187 and $A_D = 1.432$. We consider the Reynolds numbers in the range $1680 \leqslant \mathrm{Re} \leqslant 1720$. By increasing Re, the Floquet modes exhibit similar behavior with that by varying the amplitude A_D. For $1690 \leqslant \mathrm{Re} \leqslant 1705$, as shown in Figs. 11(c)–11(e), the mode A with the spanwise wave number $\beta = 9$ is the only unstable mode, while the other two Floquet modes, mode A′ and mode QP, are below the neutral line of $|\mu| = 1$. As we increase the Reynolds number to Re = 1708, as shown in Fig. 11(f), A′ changes to mode S at approximately the same wave number, and both mode S and mode B appear to be unstable, in which mode B is the dominant one with the maximum amplitude of Floquet multiplier, occurring at $\beta = 31$, and the other unstable mode, mode S, which is subharmonic, occurs at $\beta = 16$, while the third one, mode A, stays below the neutral line. We note that this sequential emergences of different instability modes is similar to that by varying the amplitude A_D.

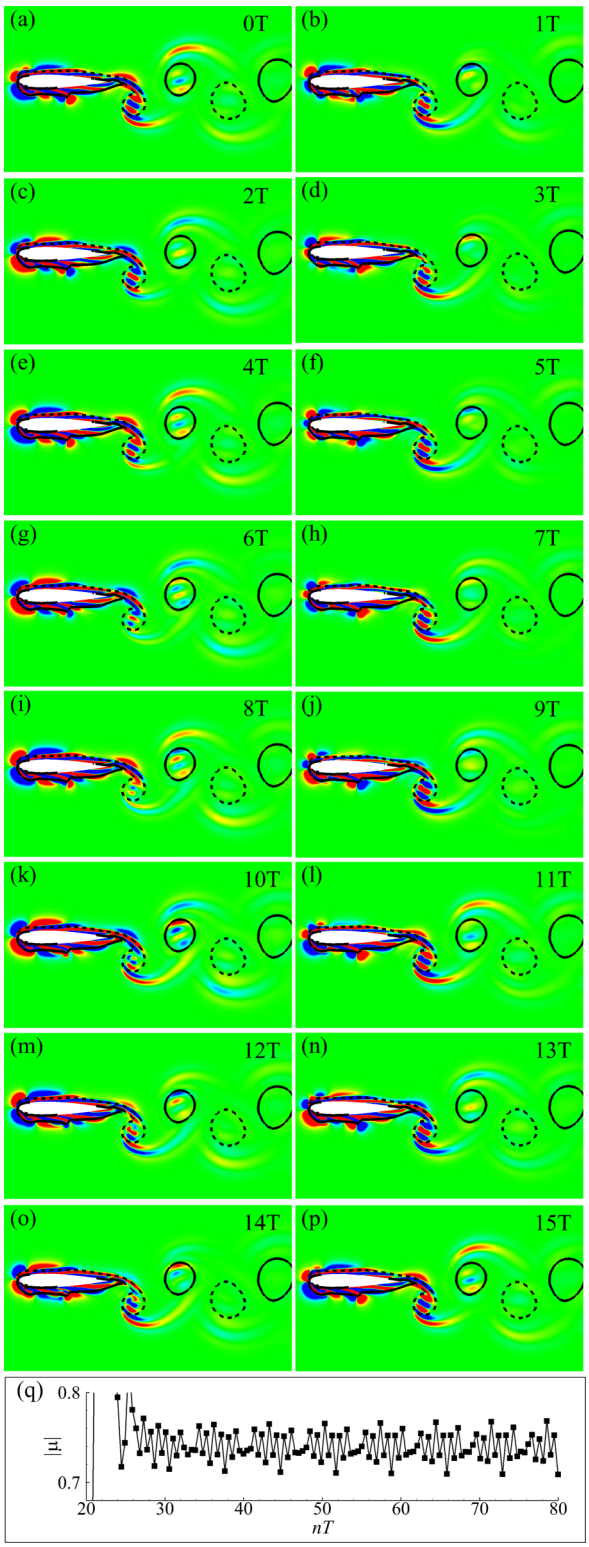

FIG. 9. [(a)–(p)] Instantaneous streamwise perturbation vorticity for mode QP of the flow past a heaving foil at Re = 1700 for (Sr, A_D) = (0.187,1.432) and $\beta = 29$. Images are set at one base-flow period apart. Blue (dark gray) and red (light gray) colors denote negative values and positive values, respectively, for continuous contours levels from −6 to 6. Spanwise vorticity contours of the base flow are also shown with solid and dashed lines for positive and negative values, respectively. (q) Time variation of $|\mu|$.

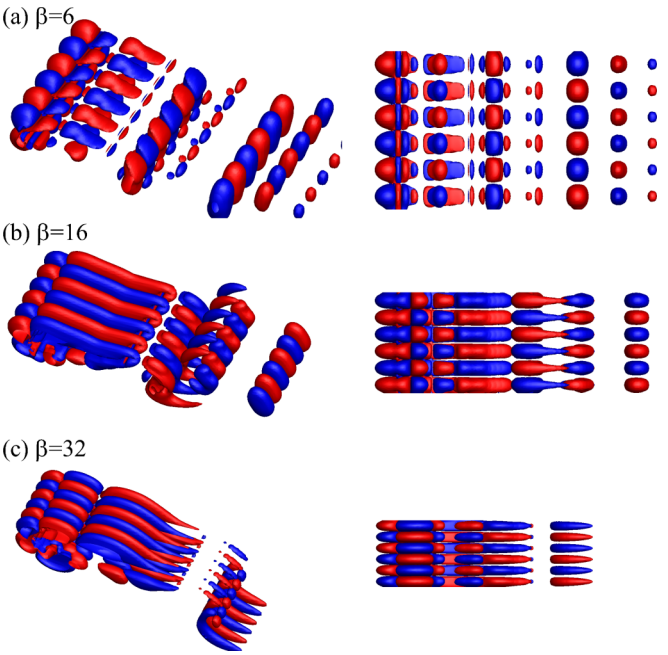

FIG. 10. Isosurfaces of the streamwise vorticity fields rebuilt from the Floquet modes for Re = 1700, (Sr, A_D) = (0.187, 1.433): (a) mode A at $\beta = 6$, (b) mode S at $\beta = 16$, and (c) mode B at $\beta = 32$. Blue (dark gray) and red (light gray) colors denote, respectively, the negative values and positive values of the vorticity.

IV. CONCLUSIONS

In this paper, Floquet stability analysis is applied to quantify the inherent three-dimensional instability arising in the wake of a periodically heaving foil. First, by using the similar hierarchy of analysis engaged in Ref. [15], we identify three key dynamical features relevant to wake vortex systems on the heaving frequency-amplitude phase space: the transition from BvK to reverse BvK vortex streets, the wake deflection, and the transition from 2D to 3D wakes. In contrast to a pitching foil, here we concentrate primarily on the distinctive characteristics for the heaving foil, particulary regarding its Floquet modes.

At a fixed Reynolds number Re = 1700, by increasing the frequency (Sr) or, equivalently, decreasing the amplitude (A_D) along the marginal stability curve in the (Sr, A_D) phase space, we observe that the critical Floquet stability mode emerges sequentially as modes A, QP, and B. It is interesting to note that both modes A and mode B are T periodic, or synchronous with respect to the base flow, in contrast to the quasiperiodic mode QP, which contains a longer secondary period.

To investigate the Floquet modes across the marginal stability curve. We fix the frequency at Sr = 0.187, of which the critical Floquet mode is located in the synchronous regime, while varying A_D around the critical value. We find that the dominant mode changes from mode A to mode B, while mode QP never becomes critical as we increase A_D. We also notice that another instability mode, mode S, arises, which is subharmonic. Physically, mode S is not realizable, because the magnitude of its Floquet multiplier is always smaller than that of mode B.

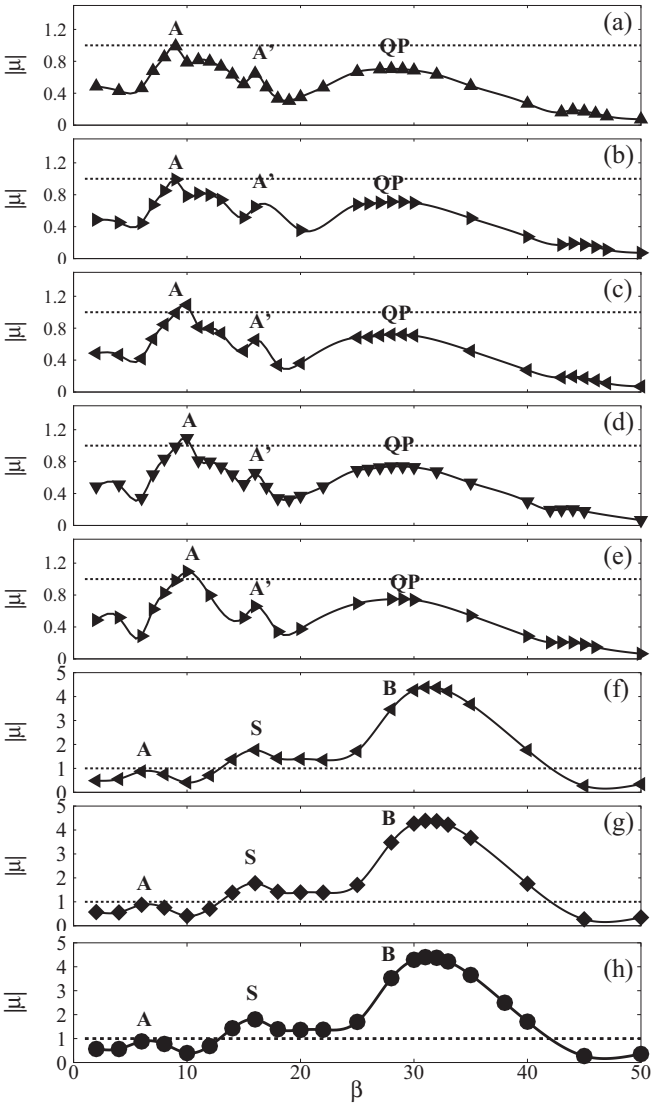

FIG. 11. Variation of Floquet multiplier magnitude $|\mu|$ with wave number β at (Sr, A_D) = (0.187, 1.432) for different Re: (a) 1680, (b) 1685, (c) 1690, (d) 1700, (e) 1705, (f) 1708, (g) 1710, and (h) 1720. The line $|\mu| = 1$ corresponds to neutral stability of the Floquet modes.

Moreover, we also consider a specific example at Sr = $0.187, A_D = 1.432$ to explore the effect of Reynolds number. As the Re increases, mode A becomes critical first. For Re up to 1708, the dominant mode switches from mode A to mode B, exhibiting behavior similar to that by varying the amplitude A_D. It is important to point out that the stability characteristics are similar for increasing Re number and that by varying A_D as crossing the transition boundary. We understand that the effect of increasing the Re number is equivalent to shifting the transition boundary to the lower left of the amplitude-frequency parametric space.

It is important to appreciate that the flow around a heaving foil differs significantly from that of a pitching foil in three-dimensional instabilities. The latter presents two unstable Floquet modes, of which only the subharmonic mode is physically realizable, while for the heaving foil, two physically realizable

modes, mode A and mode B, are identified. Both modes are synchronous with the base flow. They emerge sequentially as we increase the oscillating amplitude or increase the Reynolds number.

It is meaningful to perform fully three-dimensional direct numerical simulations to investigate if the finite-amplitude saturated forms of the Floquet modes would be consistent with the solutions from the nonlinear 3D NS equations, although it is computationally expensive.

ACKNOWLEDGMENT

This work is supported by the National Natural Science Foundation of China (Grant No. 11772299).

[1] M. Triantafyllou, G. Triantafyllou, and D. Yue, Annu. Rev. Fluid Mech. **32**, 33 (2000).
[2] S. P. Sane, J. Exp. Biol. **206**, 4191 (2003).
[3] G. K. Taylor, R. L. Nudds, and A. L. Thomas, Nature **425**, 707 (2003).
[4] L. Schouveiler, F. Hover, and M. Triantafyllou, J. Fluids Struct. **20**, 949 (2005).
[5] M. F. Platzer, K. D. Jones, J. Young, and J. S. Lai, AIAA J. **46**, 2136 (2008).
[6] I. Fenercioglu and O. Cetiner, J. Fluids Struct. **31**, 92 (2012).
[7] D. Floryan, T. Van Buren, C. W. Rowley, and A. J. Smits, J. Fluid Mech. **822**, 386 (2017).
[8] J. Anderson, K. Streitlien, D. Barrett, and M. Triantafyllou, J. Fluid Mech. **360**, 41 (1998).
[9] D. A. Read, F. Hover, and M. Triantafyllou, J. Fluids Struct. **17**, 163 (2003).
[10] R. Ramamurti and W. C. Sandberg, J. Exp. Biol. **205**, 1507 (2002).
[11] H. Dong, R. Mittal, M. Bozkurttas, and F. Najjar, AIAA Paper **81**, 2005 (2005).
[12] M. Visbal, T. O. Yilmaz, and D. Rockwell, J. Fluids Struct. **38**, 58 (2013).
[13] J. Deng, C. Caulfield, and X. Shao, Phys. Fluids **26**, 043102 (2014).
[14] J. Deng and C. P. Caulfield, Phys. Rev. E **91**, 043017 (2015).
[15] J. Deng, L. Sun, and X. Shao, Phys. Rev. E **92**, 063013 (2015).
[16] M. Moriche, O. Flores, and M. García-Villalba, Int. J. Heat Fluid Flow **62**, 44 (2016).
[17] C. Williamson, J. Fluid Mech. **328**, 345 (1996).
[18] C. H. Williamson, Annu. Rev. Fluid Mech. **28**, 477 (1996).
[19] R. Godoy-Diana, J.-L. Aider, and J. E. Wesfreid, Phys. Rev. E **77**, 016308 (2008).
[20] R. Godoy-Diana, C. Marais, J.-L. Aider, and J. E. Wesfreid, J. Fluid Mech. **622**, 23 (2009).
[21] M. M. Koochesfahani, AIAA J. **27**, 1200 (1989).
[22] K. Jones, C. Dohring, and M. Platzer, AIAA J. **36**, 1240 (1998).
[23] Z. Wei and Z. Zheng, J. Fluids Struct. **48**, 1 (2014).
[24] J. S. Lai and M. Platzer, AIAA J. **37**, 1529 (1999).
[25] K. D. von Ellenrieder and S. Pothos, Exp. Fluids **44**, 733 (2008).
[26] S. Heathcote and I. Gursul, Phys. Fluids **19**, 027104 (2007).
[27] D. J. Cleaver, Z. Wang, and I. Gursul, J. Fluid Mech. **708**, 349 (2012).
[28] D. Jallas, O. Marquet, and D. Fabre (unpublished).
[29] A. Andersen, T. Bohr, T. Schnipper, and J. H. Walther, J. Fluid Mech. **812**, R4 (2017).
[30] J. Deng, L. Sun, L. Teng, D. Pan, and X. Shao, Phys. Fluids **28**, 094101 (2016).
[31] H. Jasak, A. Jemcov, and Z. Tukovic, in *International Workshop on Coupled Methods in Numerical Dynamics* (Dubrovnik, Croatia, 2007), Vol. 1000, pp. 1–20.
[32] J. H. Ferziger and M. Perić, *Computational Methods for Fluid Dynamics*, Vol. 3 (Springer, Berlin, 2002).
[33] G. Iooss, D. D. Joseph, F. Jehring, and P. Halmos, *Elementary Stability and Bifurcation Theory*, Vol. 34 (Springer, Berlin, 1980).
[34] P. J. Schmid and D. S. Henningson, *Stability and Transition in Shear Flows*, Vol. 142 (Springer, Berlin, 2001).
[35] D. Barkley and R. D. Henderson, J. Fluid Mech. **322**, 215 (1996).
[36] D. Barkley, L. S. Tuckerman, and M. Golubitsky, Phys. Rev. E **61**, 5247 (2000).
[37] H. M. Blackburn and J. Lopez, Phys. Fluids **15**, L57 (2003).
[38] J. Robichaux, S. Balachandar, and S. Vanka, Phys. Fluids **11**, 560 (1999).
[39] D. Richter, E. S. Shaqfeh, and G. Iaccarino, J. Non-Newtonian Fluid Mech. **166**, 554 (2011).
[40] J. Deng, L. Sun, and X. Shao, Phys. Fluids **29**, 094104 (2017).
[41] J. R. Elston, J. Sheridan, and H. M. Blackburn, Eur. J. Mech. B Fluids **23**, 99 (2004).
[42] J. R. Elston, H. M. Blackburn, and J. Sheridan, J. Fluid Mech. **550**, 359 (2006).
[43] G. J. Sheard, M. J. Fitzgerald, and K. Ryan, J. Fluid Mech. **630**, 43 (2009).